Letter

Topological phase transition driven by magnetic field and topological Hall effect in an antiferromagnetic skyrmion lattice

M. Tomé[1,2] and H. D. Rosales[1,2,3,*]

[1]*Instituto de Física de Líquidos y Sistemas Biológicos (IFLYSIB), UNLP-CONICET, Facultad de Ciencias Exactas, La Plata, Argentina*

[2]*Departamento de Física, Facultad de Ciencias Exactas, Universidad Nacional de La Plata, La Plata, Argentina*

[3]*Departamento de Cs. Básicas, Facultad de Ingeniería, Universidad Nacional de La Plata, C.C. 67, 1900 La Plata, Argentina*

(Received 29 September 2020; accepted 16 December 2020; published 6 January 2021)

The topological Hall effect (THE), given by a composite of electric and topologically nontrivial spin texture is commonly observed in magnetic skyrmion crystals. Here we present a study of the THE of electrons coupled to antiferromagnetic skyrmion lattices (AF-SkX). We show that, in the strong Hund coupling limit, topologically nontrivial phases emerge at specific fillings. Interestingly, at low filling an external field controlling the magnetic texture drives the system from a conventional insulator phase to a phase exhibiting the THE. Such behavior suggests the occurrence of a topological transition which is confirmed by a closing of the bulk gap that is followed by its reopening, appearing simultaneously with a single pair of helical edge states. This transition is further verified by the calculation of the Chern numbers and Berry curvature. We also compute a variety of observables in order to quantify the THE, namely, Hall conductivity and the orbital magnetization of electrons moving in the AF-SkX texture.

DOI: 10.1103/PhysRevB.103.L020403

Introduction. Magnetic skyrmions, a kind of topologically protected soliton, are nanometer size spin textures that have been shown to be of great practical interest due to both their fundamental properties and their promising potential in spintronics-based applications [1,2]. They have been evidenced experimentally in a wide variety of materials including chiral magnets such as MnSi [3,4], FeGe [5], $Fe_xCo_{1-x}Si$ [6], and β-Mn-type Co-Zn-Mn [7] and insulator materials such as Cu_2OSeO_3 [8,9]. In most cases, periodic arrays of skyrmions are stabilized by the competition of strong ferromagnetic exchange interactions, the external magnetic field, and the antisymmetric Dzyaloshinskii-Moriya (DM) interaction [10–13]. However, in recent years, theoretical studies have suggested that skyrmions might be also stabilized in antiferromagnets where frustration helps to stabilize antiferromagnetic skyrmion crystals (AF-SkX) consisting of multiple interpenetrated ferromagnetic skyrmion lattices [14–22]. Recently, in the spinel $MnSc_2S_4$, the first realization of an AF-SkX (fractional)-like structure has been discovered, where the planes (triangular lattices) perpendicular to the field direction host interpenetrated fractional ferromagnetic skyrmion lattices [23].

When conduction electrons are coupled to the local magnetic background, they accumulate a Berry phase as they travel through the skyrmions' spin configuration which acts as a local effective magnetic field leading to the topological Hall effect (THE) [24–31]. Most of the previous studies on THE have focused on systems consisting of ferromagnetic SkX showing unconventional behavior that emerges as a consequence of the nontrivial smooth magnetic texture [32–34]. However, a not so desired feature of skyrmions hosted in ferromagnets is that they exhibit an inevitable topology effect, namely, the skyrmion Hall effect [35]. In this phenomena, the magnetic skyrmions do not move collinear to the current flow direction, but acquire a transverse motion due to the appearance of a topological Magnus force acting upon the nonzero topological charge. To avoid this disadvantage, theoretical studies have suggested that the skyrmion Hall effect can be suppressed by utilizing the counterpart of the ferromagnetic skyrmions, the antiferromagnetic skyrmions, which are also topologically protected but without showing the skyrmion Hall effect [36]. In this context, electrons coupled to antiferromagnetic skyrmion lattices have been less explored, even knowing that the multiple sublattice structure can induce interesting magnetic phenomena [37]. Therefore a question that arises naturally is whether conduction electrons coupled to this kind of skyrmion lattice could present exotic new physics.

This Letter addresses this relevant question on the THE of electrons in topologically nontrivial AF-SkX textures on the triangular lattice. By means of extensive Monte Carlo simulations and exact diagonalization for the magnetic and fermionic sector, respectively, we find that, in the strong Hund coupling limit, at low filling it is possible to control the THE and its protected edge states by tuning the external magnetic field. This phenomena is confirmed by a closing and further reopening of the bulk gap and the transition from trivial to nontrivial Chern number. As a complement, we have computed the orbital magnetization, which is directly related to the Berry-phase effect, showing surprisingly opposite signs at both sides of the topological transition. This property enables a "switch" on/off of the THE and orbital magnetization by an external magnetic field.

*Corresponding author: rosales@fisica.unlp.edu.ar

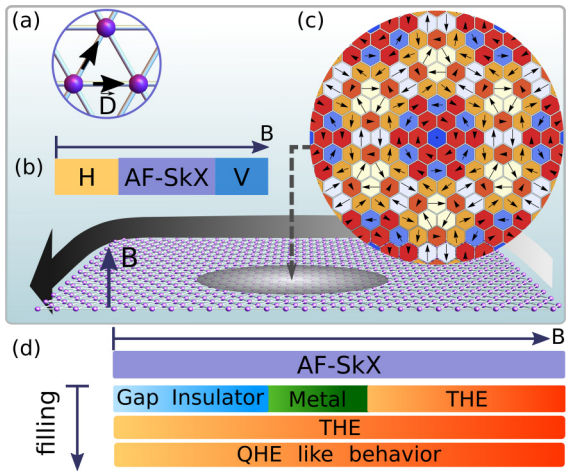

FIG. 1. (a) DM interactions **D** (black arrows). (b) Low-temperature phase diagram of the magnetic Hamiltonian in Eq. (2) including helical (H), AF-SkX, and vortex-like (V) phases. (c) Portion of an AF-SkX magnetic background considered in this Letter for $D/J = 0.5$ and $B/J = 4.6$. (d) Schematic phase diagram of the electronic Hamiltonian in Eq. (3). At low filling, the magnetic field induces a sequence of topological transitions: band insulator → metal → THE; at high filling the system's behavior can be connected with the integer quantum Hall effect.

Model and methods. In this work we consider a tight-binding model on a triangular lattice where the interaction of electrons with an AF-SkX texture is described by the following Hamiltonian:

$$H = -\sum_{\langle \mathbf{r},\mathbf{r}'\rangle,\sigma} t_{\mathbf{r}\mathbf{r}'}\,(\hat{c}^{\dagger}_{\mathbf{r}\sigma}\hat{c}_{\mathbf{r}',\sigma} + \text{H.c.}) - J_h \sum_{\mathbf{r},\mu\nu} \mathbf{S}_{\mathbf{r}}\cdot\mathbf{s}_{\mathbf{r}}, \qquad (1)$$

where $\hat{c}_{\mathbf{r}\sigma}$ ($\hat{c}^{\dagger}_{\mathbf{r}\sigma}$) is the creation (annihilation) operator at the site $\mathbf{r}$ with spin ($\sigma = \uparrow, \downarrow$), $t_{\mathbf{r}\mathbf{r}'}$ is the hopping between nearest-neighbor sites, and J_H is the Hund's coupling strength between the electron spin $\mathbf{s}_{\mathbf{r}} = \frac{1}{2}\hat{c}^{\dagger}_{\mathbf{r},\mu}\vec{\sigma}^{\mu\nu}\hat{c}_{\mathbf{r},\nu}$ and the magnetic background $\mathbf{S}_{\mathbf{r}}$. In order to include a spin texture made of an AF-SkX phase we perform Monte Carlo simulations with overrelaxation updates [14,38] for system sizes of $N = L^2$ sites ($L = 12$–84) and periodic-boundary conditions on the following pure magnetic Hamiltonian [14,39] (see the Supplemental Material [40], Sec. I, for more details on the simulations):

$$H_S = \sum_{\langle \mathbf{r},\mathbf{r}'\rangle} J\,\mathbf{S}_{\mathbf{r}}\cdot\mathbf{S}_{\mathbf{r}'} + \mathbf{D}_{\mathbf{r}\mathbf{r}'}\cdot(\mathbf{S}_{\mathbf{r}}\times\mathbf{S}_{\mathbf{r}'}) - B\sum_{\mathbf{r}} S^{z}_{\mathbf{r}}, \qquad (2)$$

where J and $\mathbf{D}_{\mathbf{r}\mathbf{r}'} = D(\mathbf{r}'-\mathbf{r})/\|\mathbf{r}'-\mathbf{r}\|$ are the antiferromagnetic and DM nearest neighbor couplings, respectively [see Fig. 1(a)], and B is the strength of the magnetic field along the z axis. We consider $D/J = 0.5$ for the rest of the Letter as a representative value [14,39] where it is known from the model in Eq. (2) that an AF-SkX emerges consisting of the superposition of three interpenetrated ferromagnetic skyrmion lattices [14,39] [Fig. 1(c)] corresponding to a portion of the lattice for $B/J = 4.6$ (see the Supplemental Material [40], Sec. I).

In a recent work it was shown that the mixed dynamics of both electrons and spins tend to stabilize the AF-SkX phase in the adiabatic regime $J_H/t \gg 1$ [41], allowing us to fix the magnetic texture in Eq. (1) throughout our calculations. With this in mind, let us focus on this regime $J_H/t \gg 1$, where the spin of the electrons are aligned parallel to the local moment and the low-energy physics can be described by an effective Hamiltonian of spinless fermions as in Ref. [42] (see Supplemental Material [40], Sec. II, for details):

$$H_{\text{eff}} = \sum_{\mathbf{r},\mathbf{r}'} t^{\text{eff}}_{\mathbf{r}\mathbf{r}'}\hat{d}^{\dagger}_{\mathbf{r}}\hat{d}_{\mathbf{r}'}, \qquad (3)$$

where $\hat{d}^{\dagger}_{\mathbf{r}}$ ($\hat{d}_{\mathbf{r}}$) is the creation (annihilation) operator, $\cos\theta_{\mathbf{r}\mathbf{r}'} = \mathbf{S}_{\mathbf{r}}\cdot\mathbf{S}_{\mathbf{r}'}$, $t^{\text{eff}}_{\mathbf{r}\mathbf{r}'} = t_{\mathbf{r}\mathbf{r}'}\cos(\theta_{\mathbf{r}\mathbf{r}'}/2)e^{i\,a_{\mathbf{r}\mathbf{r}'}}$ is the effective hopping amplitude, and the phase $\tan(a_{\mathbf{r}\mathbf{r}'}) = -\sin(\phi_{\mathbf{r}}-\phi_{\mathbf{r}'})/[\cos(\phi_{\mathbf{r}}-\phi_{\mathbf{r}'}) + \cot(\theta_{\mathbf{r}}/2)\cot(\theta_{\mathbf{r}'}/2)]$.

The electronic band structure and other quantities of interest are obtained through numerical diagonalization of the resulting Hamiltonian matrix in the reciprocal space. Therefore, once the eigenvector $|u_n(\mathbf{k})\rangle$ and the eigenenergies $\epsilon_n(\mathbf{k})$ are determined, we calculate the Hall conductivity σ_{xy} by means of the standard Kubo formula, which at $T = 0$, reduces to

$$\sigma_{xy} = \frac{e^2}{2\pi h}\sum_n \int \Theta(\epsilon_n - \epsilon_F)\Omega^{(n)}_{xy}\,d^2k, \qquad (4)$$

where the Berry curvature for the band n is $\Omega^{(n)}_{ab} = 2\sum_{m\neq n}\text{Im}[v_a]^{nm}[v_b]^{mn}/(\epsilon_m-\epsilon_n)^2$, ϵ_F is the Fermi energy, and $[v_a]^{nm} = \langle u_n|v_a|u_m\rangle$ ($a = x, y$) is the matrix element of the velocity operator $\mathbf{v} = \frac{i}{\hbar}[H_{\text{eff}}, \mathbf{R}]$, with the position operator being $\mathbf{R} = \sum_{\mathbf{r}}\mathbf{r}\,d^{\dagger}_{\mathbf{r}}d_{\mathbf{r}}$. When the Fermi energy ϵ_F lies inside a band gap, the Hall conductivity is quantized as $\sigma_{xy} = e^2/h\sum_n C_n$, where the integers C_n are the so-called Chern numbers. Relevant Chern numbers are calculated independently of σ_{xy} through the Fukui-Hatsugai numerical method [43]. Thus, due to the bulk-boundary correspondence principle [44], in an open-boundary system one would expect to find a number $|\nu|$ of topologically protected chiral edges states crossing the nth band gap, where $\nu = \sum_n C_n$. In addition, we also calculate the out-of-plane component of the orbital magnetization [45–47]

$$\begin{aligned}\mathcal{M}^z &= \mathcal{M}_c + \mathcal{M}_t \\ &= \frac{1}{(2\pi)^2}\sum_n \int_{\text{BZ}} \Theta_n\, m^z_n\, d^2k \\ &\quad + \frac{e}{4\pi h}\sum_n \int_{\text{BZ}} \Theta_n\big(\Omega^{(n)}_{xy} - \Omega^{(n)}_{yx}\big)(\epsilon_F - \epsilon_n)d^2k, \end{aligned} \qquad (5)$$

where $\Theta_n = \Theta(\epsilon_n - \epsilon_F)$ is the Heaviside step function, and $m^c_n = -\frac{e}{2\hbar}\sum_{m\neq n}\epsilon^{abc}\text{Im}[v_a]^{nm}[v_b]^{mn}/(\epsilon_m-\epsilon_n)$ is the crystal orbital magnetic moment with ϵ^{abc} being the Levi-Civita tensor (summation over a and b is implicit). $\mathcal{M}_c$ corresponds to the contribution from the intrinsic orbital moment (conventional part), whereas $\mathcal{M}_t$ corresponds to corrections of a topological nature.

Band structure and topological phase transition. In Fig. 2(a) we show a typical band structure obtained in the presence of an AF-SkX background. Here we identify two main distinct energy regions: (i) a low-energy sector consisting of strongly overlapping bands except for a field-dependent

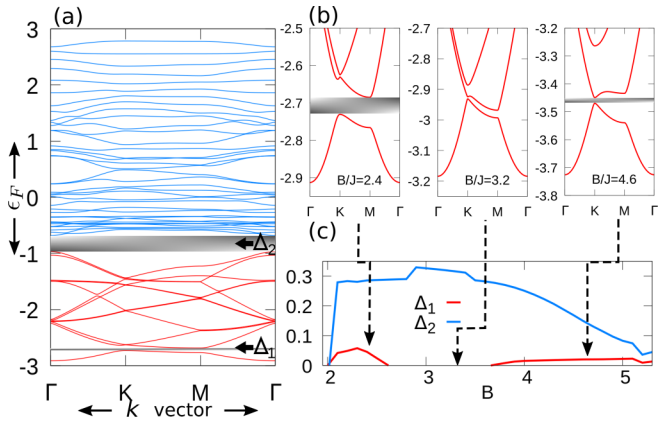

FIG. 2. (a) Representative band structure of the model in Eq. (3) for $B/J = 2.4$ (energy in units of t). Red and blue sets of curves indicate the two regions with different properties. The gray-shaded areas mark the two relevant gaps of the system. (b) Closing and further reopening of the bulk gap Δ_1. (c) Evolution of the gaps Δ_1 and Δ_2 vs the magnetic field B.

global bulk gap Δ_1 between the first and second bands (red curves), and (ii) a high-energy sector resembling a typical THE spectrum in the presence of a ferromagnetic skyrmion background [32] (blue curves). Both sectors are separated by a persistent energy gap, Δ_2 [see Fig. 1(c)].

In this section, we focus our attention on the low-energy sector, leaving the discussion of the high-energy sector to the next section. For sequentially bigger fields it is found that the overlapping region barely changes. Figure 2(b) shows a closing and further reopening of the first bulk gap Δ_1 for increasing fields. These two sectors where Δ_1 is nonzero (at low field and a high field) are well separated by a broad gapless region as shown in Fig. 2(c). Upon further inspection we finds a noticeable change in both the Hall conductivity and the orbital magnetization when the Fermi energy sits inside the band gap. In Fig. 3 we show these quantities for low field (left panels) and high field (right panels) displaying a transition from $\sigma_{xy} = 0$ at low field to a quantized value

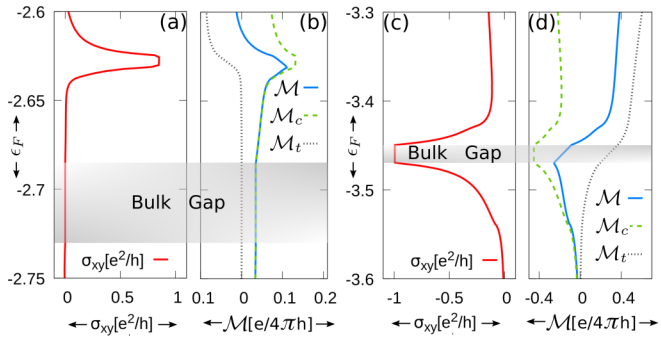

FIG. 3. ϵ_F dependence (in units of t) of the topological Hall conductivity σ_{xy} [panels (a) and (c)], exhibiting a transition from zero to quantized value in the bulk gap window as a function of Fermi energy. Panels (b) and (d) show the orbital magnetization $\mathcal{M}$ (and $\mathcal{M}_c$, $\mathcal{M}_t$) in units of $[e/4\pi\, h]$. The shaded areas correspond to the energy gap Δ_1.

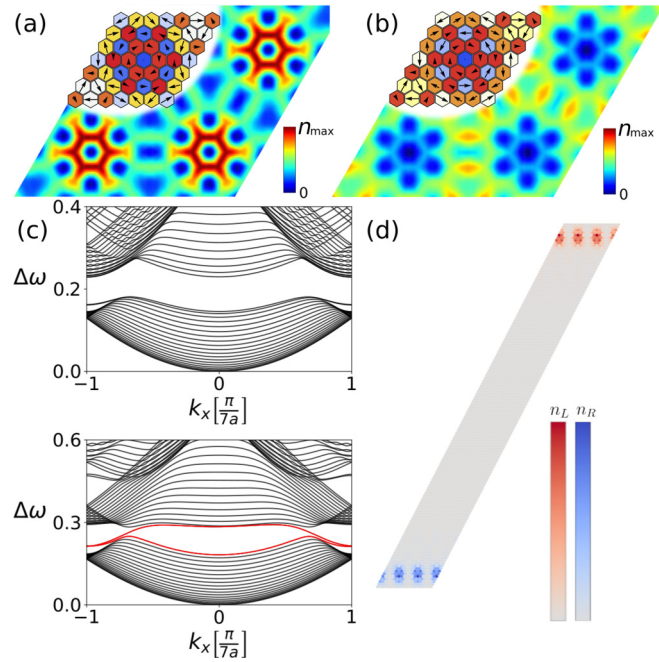

FIG. 4. Electronic occupation at the Γ point for the lowest band for $B/J = 2.4$ (a) and $B/J = 4.6$ (b). In the trivial case ($C_1 = 0$) the electron density is strongly localized inside the AF skyrmion; when $C_1 = -1$ it becomes delocalized (the top-left insets show the spin configurations). (c) One-dimensional band structure ($\Delta w = \epsilon_n - \epsilon_1$ in units of t) for a nanoribbon geometry with periodic-boundary (upper) and open-boundary (bottom) conditions. In the last case, the edge state (red curve) is clearly observed between the two adjacent bands, which demonstrates a nonzero Chern number. (d) The edges states are localized at the boundary (top and bottom) of the nanoribbon.

$\sigma_{xy} = -\frac{e^2}{h}$ at high field [Figs. 3(a) and 3(c)]. This is confirmed by the calculation of the Chern number where the lowest band is topologically trivial with $C_1 = 0$ at low field and nontrivial with $C_1 = -1$ at high field. This topological change is also evidenced in the orbital magnetization [Eq. (6)]. In Figs. 3(b) and 3(d) we show the orbital magnetization ($\mathcal{M}$) and its two components, $\mathcal{M}_c$ and $\mathcal{M}_t$, as a function of ϵ_F. On one hand, we observe that, in the energy gap, at low field there is only a negative contribution from the conventional part $\mathcal{M}_c$. Because $C_1 = 0$ we have $\mathcal{M}_t \equiv 0$. On the other hand, at high field, $\mathcal{M}_c$ keeps constant inside the gap, due to the fact that the integral of m_n^z does not depend on ϵ_F. In contrast, the Berry-phase term $\mathcal{M}_c$ linearly increases with ϵ_F, as is expected from Eq. (6).

In order to inspect in more detail the effects of the transition, we calculate the electronic occupation $n_{\mathbf{r}} = \langle u_1(\mathbf{k})|\hat{d}_{\mathbf{r}}^\dagger \hat{d}_{\mathbf{r}}|u_1(\mathbf{k})\rangle$ within the unit cell at the Γ point for the lowest band for $B/J = 2.4$ and 4.6. In the low-field region it is strongly confined around the antiferromagnetic skyrmion center in a ringlike configuration [48] [Fig. 4(a)]. As we cross the transition the electronic occupation spreads out, getting away from the skyrmions' centers, forming a connected configuration throughout the system [Fig. 4(b)]. This localized/delocalized type transition is compatible with the change in Hall conductivity.

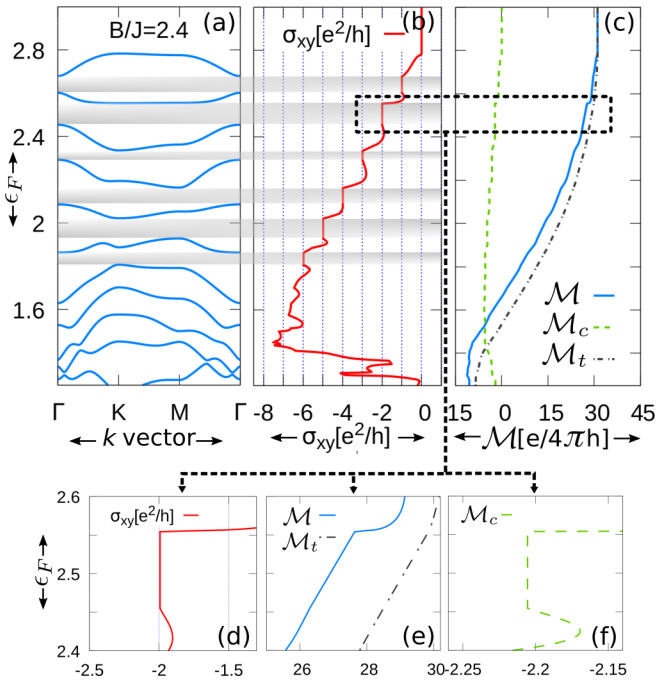

FIG. 5. (a) Electronic band structure at the high-filling band (in units of t), (b) Hall conductivity, and (c) orbital magnetization as a function of the Fermi energy (vertical axis). Regions with bulk gap are indicated by a gray rectangular box. In panels (d)–(f), we show a zoomed-in region in order to highlight the connection between quantities.

Last, we study the presence of in-gap chiral edge states. To this end, we have numerically diagonalized the Hamiltonian Eq. (3) in a one-dimensional strip configuration with a width of 20 unit cells. The calculated band structure with periodic- and open-boundary conditions is shown in Fig. 4(c). In the high-field region, a gap-crossing edge state, absent in the low-field region, is observed. The electronic occupation for this state localizes in the edge of the sample, as shown in Fig. 4(d). A similar behavior can be found in the persistent energy gap Δ_2 with stable in-gap chiral edge states (see the Supplemental Material [40], Sec. II, Fig. 2). This result agrees with the bulk-boundary correspondence principle.

Therefore, a system of this kind with a filled first band could be tuned from an insulator to a metal to a Chern insulator phase by changing the external magnetic field. Edge conducting states can be turned on and off in the same manner.

High-filling sector. At high filling, the band structure, Hall conductivity, and orbital magnetization show a striking similarity to thosw observed in ferromagnetic skyrmion crystals [32,49] as functions of the Fermi energy (see Fig. 5). The presence of the THE is a consequence of the three-sublattice structure of the AF-SkX magnetic background. On an AF-SkX on a bipartite lattice, one would expect the emergent field to fluctuate around zero, leading to a vanishing Hall conductivity [37]. However, in the case of the AF-SkX on the triangular lattice, the emergent field fluctuates around a nonzero value and its strength is comparable to that of the emergent field coming from a ferromagnetic skyrmion lattice background. In this sense, a correspondence between the integer quantum Hall effect and the THE on the AF-SkX can be traced, as is the case with ferromagnetic skyrmion lattices [32].

Conclusions. In this Letter we have studied the topological Hall effect and orbital magnetism of electrons coupled to an antiferromagnetic skyrmion lattice. The band structure consists of two energy regions, separated by a persistent energy gap. The low-energy sector consists of strongly overlapping bands except for a switchable bulk gap between the first and second bands. The high-energy sector shows a striking similarity to that of the integer quantum Hall effect.

At low filling, we found that a magnetic field drives the system from a conventional insulating state to a topological insulator state hosting chiral edge states in generic strip geometries. This topological change is clearly manifested in the Chern numbers, the electron density, the Hall conductivity, and the orbital magnetization. In the region with Chern number $C_1 = 0$, the electron density is strongly localized at the AF-skyrmion cores forming a ringlike distribution. In the region with $C_1 = -1$, it becomes delocalized. We found that the localization/delocalization of the ring states can be controlled by the magnetic field which determines the texture details. The Hall conductivity presents a switchable behavior from a null to a quantized value of $\sigma_{xy} = -e^2/h$ when the Fermi energy is inside the bulk gap. We have found that the two parts, $\mathcal{M}_c$ and $\mathcal{M}_t$, of the orbital magnetization display fully different behaviors in the $C_1 = 0$ and $C_1 = -1$ regions because of their different roles in these two regions.

At high fillings, even having a three-sublattice structure of the AF-SkX we recover a behavior similar to that observed in a ferromagnetic skyrmion lattice where it is possible to connect the THE with the integer quantum Hall effect.

Our results highlight the richness of the electronic phases arising from systems hosting AF-SkX states and their potential as platforms for spintronic devices. The present study on the THE in antiferomagnetic skyrmion lattices calls for experimental verification. The low-filling topological phase transition and controlled chiral edge states can be studied in materials which exhibit an AF-SkX phase, e.g., the recent fractional skyrmion lattice observed in the compound $MnSc_2S_4$ [23]. In this material, the magnetic ions Mn^{2+} form a diamond lattice. At low temperature and finite magnetic field, each triangular lattice layer along the [111] direction realizes a fractional AF-SkX that is composed of three ferromagnetic skyrmion sublattices.

Acknowledgments. We thank Pierre Pujol for valuable comments. H.D.R thanks Flavia Gómez Albarracín for fruitful discussions. This work was partially supported by CONICET (Grant No. PIP 2015-813), ANPCyT (Grant No. PICT 2012-1724), and SECyT-UNLP (Grant No. PPID X039). H.D.R. acknowledges support from ANPCyT (Grant No. PICT 2016-4083).

[1] N. Nagaosa and Y. Tokura, Nat. Nanotechnol. **8**, 899 (2013).

[2] A. Fert, V. Cros, and J. Sampaio, Nat. Nanotechnol. **8**, 152 (2013).

[3] S. Mühlbauer, B. Binz, F. Jonietz, C. Pfleiderer, A. Rosch, A. Neubauer, R. Georgii, and P. Böni, Science **323**, 915 (2009).

[4] F. Jonietz, S. Mühlbauer, C. Pfleiderer, A. Neubauer, W. Münzer, A. Bauer, T. Adams, R. Georgii, P. Böni, R. A. Duine *et al.*, Science **330**, 1648 (2010).

[5] X. Yu, N. Kanazawa, Y. Onose, K. Kimoto, W. Zhang, S. Ishiwata, Y. Matsui, and Y. Tokura, Nat. Mater. **10**, 106 (2011).

[6] X. Yu, Y. Onose, N. Kanazawa, J. Park, J. Han, Y. Matsui, N. Nagaosa, and Y. Tokura, Nature (London) **465**, 901 (2010).

[7] Y. Tokunaga, X. Yu, J. White, H. M. Rønnow, D. Morikawa, Y. Taguchi, and Y. Tokura, Nat. Commun. **6**, 7638 (2015).

[8] S. Seki, X. Yu, S. Ishiwata, and Y. Tokura, Science **336**, 198 (2012).

[9] S. Seki, S. Ishiwata, and Y. Tokura, Phys. Rev. B **86**, 060403(R) (2012).

[10] A. N. Bogdanov and D. A. Yablonskii, Zh. Eksp. Teor. Fiz. **95**, 178 (1989).

[11] A. Bogdanov and A. Hubert, J. Magn. Magn. Mater. **138**, 255 (1994).

[12] A. Bocdanov and A. Hubert, Phys. Status Solidi B **186**, 527 (1994).

[13] U. K. Roessler, A. Bogdanov, and C. Pfleiderer, Nature (London) **442**, 797 (2006).

[14] H. D. Rosales, D. C. Cabra, and P. Pujol, Phys. Rev. B **92**, 214439 (2015).

[15] J. Barker and O. A. Tretiakov, Phys. Rev. Lett. **116**, 147203 (2016).

[16] X. Zhang, Y. Zhou, and M. Ezawa, Sci. Rep. **6**, 24795 (2016).

[17] H. Fujita and M. Sato, Phys. Rev. B **95**, 054421 (2017).

[18] C. Jin, C. Song, J. Wang, and Q. Liu, Appl. Phys. Lett. **109**, 182404 (2016).

[19] S. A. Osorio, H. D. Rosales, M. B. Sturla, and D. C. Cabra, Phys. Rev. B **96**, 024404 (2017).

[20] S. A. Osorio, M. B. Sturla, H. D. Rosales, and D. C. Cabra, Phys. Rev. B **99**, 064439 (2019).

[21] S. A. Osorio, M. B. Sturla, H. D. Rosales, and D. C. Cabra, Phys. Rev. B **100**, 220404(R) (2019).

[22] M. E. Villalba, F. A. Gómez Albarracín, H. D. Rosales, and D. C. Cabra, Phys. Rev. B **100**, 245106 (2019).

[23] S. Gao, H. D. Rosales, F. A. Gómez Albarracín, V. Tsurkan, G. Kaur, T. Fennell, P. Steffens, M. Boehm, P. Čermák, A. Schneidewind, E. Ressouche, D. C. Cabra, C. Rüegg, and O. Zaharko, Nature (London) **586**, 37 (2020).

[24] A. Neubauer, C. Pfleiderer, B. Binz, A. Rosch, R. Ritz, P. G. Niklowitz, and P. Böni, Phys. Rev. Lett. **102**, 186602 (2009).

[25] T. Schulz, R. Ritz, A. Bauer, M. Halder, M. Wagner, C. Franz, C. Pfleiderer, K. Everschor, M. Garst, and A. Rosch, Nat. Phys. **8**, 301 (2012).

[26] N. Kanazawa, Y. Onose, T. Arima, D. Okuyama, K. Ohoyama, S. Wakimoto, K. Kakurai, S. Ishiwata, and Y. Tokura, Phys. Rev. Lett. **106**, 156603 (2011).

[27] M. Lee, W. Kang, Y. Onose, Y. Tokura, and N. P. Ong, Phys. Rev. Lett. **102**, 186601 (2009).

[28] Y. Li, N. Kanazawa, X. Z. Yu, A. Tsukazaki, M. Kawasaki, M. Ichikawa, X. F. Jin, F. Kagawa, and Y. Tokura, Phys. Rev. Lett. **110**, 117202 (2013).

[29] P. Bruno, V. K. Dugaev, and M. Taillefumier, Phys. Rev. Lett. **93**, 096806 (2004).

[30] P. B. Ndiaye, C. A. Akosa, and A. Manchon, Phys. Rev. B **95**, 064426 (2017).

[31] H. D. Rosales, F. A. Gómez Albarracín, and P. Pujol, Phys. Rev. B **99**, 035163 (2019).

[32] B. Göbel, A. Mook, J. Henk, and I. Mertig, Phys. Rev. B **95**, 094413 (2017).

[33] B. Göbel, A. Mook, J. Henk, and I. Mertig, New J. Phys. **19**, 063042 (2017).

[34] B. Göbel, A. Mook, J. Henk, and I. Mertig, Eur. Phys. J. B **91**, 179 (2018).

[35] W. Jiang, X. Zhang, G. Yu, W. Zhang, X. Wang, M. B. Jungfleisch, J. E. Pearson, X. Cheng, O. Heinonen, K. L. Wang *et al.*, Nat. Phys. **13**, 162 (2017).

[36] B. Göbel, I. Mertig, and O. A. Tretiakov, Phys. Rep. (2020), doi: 10.1016/j.physrep.2020.10.001.

[37] B. Göbel, A. Mook, J. Henk, and I. Mertig, Phys. Rev. B **96**, 060406 (2017).

[38] F. A. Gómez Albarracín and H. D. Rosales, Phys. Rev. B **93**, 144413 (2016).

[39] S. A. Díaz, J. Klinovaja, and D. Loss, Phys. Rev. Lett. **122**, 187203 (2019).

[40] See Supplemental Material at http://link.aps.org/supplemental/10.1103/PhysRevB.103.L020403 for details related to the Monte Carlo simulations, the spin configurations, and the magnetic unit cells used for our calculations (Sec. I); the details of the transformation to obtain the effective Hamiltonian of spinless fermions (Sec. II); and figures of the electronic occupation in the energy gap Δ_2 (Sec. III).

[41] S. Reja, arXiv:2005.02724.

[42] K. Ohgushi, S. Murakami, and N. Nagaosa, Phys. Rev. B **62**, R6065 (2000).

[43] T. Fukui, Y. Hatsugai, and H. Suzuki, J. Phys. Soc. Jpn. **74**, 1674 (2005).

[44] Y. Hatsugai, Phys. Rev. Lett. **71**, 3697 (1993).

[45] M.-C. Chang and Q. Niu, Phys. Rev. B **53**, 7010 (1996).

[46] D. Xiao, J. Shi, and Q. Niu, Phys. Rev. Lett. **95**, 137204 (2005).

[47] A. Raoux, F. Piéchon, J.-N. Fuchs, and G. Montambaux, Phys. Rev. B **91**, 085120 (2015).

[48] M. Redies, F. Lux, J.-P. Hanke, P. Buhl, S. Blügel, and Y. Mokrousov, Phys. Rev. B **102**, 184407 (2020).

[49] K. Hamamoto, M. Ezawa, and N. Nagaosa, Phys. Rev. B **92**, 115417 (2015).